RESEARCH ARTICLE

Electronic Properties of the Chalcopyrites $AgFeS_2$, $AgFeSe_2$ and $AgFeTe_2$ Compounds

N. N. Omehe[1], D. N. Nwachuku[2,*]

[1]Physics Department, Federal University Otuoke, Bayelsa State, Nigeria
[2]Physics Department, College of Education, Agbor Delta State, Nigeria

*Corresponding author: E-mail: ngozinwachuku1@gmail.com

DOI: 10.5185/amlett.2021.011597

The electronic properties of the Chalcopyrites $AgFeS_2$, $AgFeSe_2$ and AgFeTe2 have been investigated using the pseudopotential method within the density functional theory (DFT). The LDA+U technique and the projector augmented waves (PAW) were used for the electronic band structure calculations, while the norm-conserving pseudopotentials were used for the structure optimization. The calculated results showed that $AgFeS_2$, $AgFeSe_2$ and $AgFeTe_2$ are semiconductors with energy bandgap values of 3.33 eV, 0.05 eV and 1.30 eV respectively. The transition points in the band structure were all notable because of the narrowness of the bands about the Fermi level. The total density of states and their corresponding partial density of states were also computed.

Introduction

Ternary I-III-VI_2 semiconductors are regarded as the most promising materials for thin-film technology because of their unique optoelectronic properties such as large absorption coefficients, high conversion efficiencies, low toxicity of components and narrow energy bandgap values [**1,2**]. For over a decade, semiconducting compounds containing earth-abundant and non-toxic elements like Cu, Zn, Sn, S and Se are being used as thin-film photovoltaic (PV) absorbers, replacing the more conventional materials like In, Si, Ge, Cd and Te, which are not environmental friendly and some are not readily available. There are numerous experimental and theoretical works in these compounds and it has been well known for many years that their electrical properties often vary dramatically with composition [**3,4**]. According to Gershon *et. al.,* [**5**], the performance of CZTSSe-based devices lags behind CIGS due to theirlimited open-circuit voltages. Material analysis also revealed that components of Cu and Zn contain a large density of Cu/Zn anti-site pairs, resulting in almost disorder on the Cu/Zn atomic plane in the material [**6**]. In recent times, Silver Chalcopytes (Ag^+) have been studied particularly because of their high ionic conductivity in high temperature structures [**7**]. Although Ag^+ is not considered to be earth-abundant, its use is not likely to limit the implementation in PV materials, according to Gershon *et. al.,* [**8**].

The compounds $AgFeS_2$, $AgFeSe_2$ and $AgFeTe_2$ are novel ternary I-III-VI_2 semiconductors characterized by Ag in different types of coordination by Chalcopytes and by Ag-Ag distances that are only slightly larger than the metal, Fe. Inclusion of Fe into the compounds allow for low bandgaps because of the presence of Fe *3d*- orbitals within the expected bandgaps [**9**]. These compounds could be in solid form at room temperature as well as in liquid form when heated or they can be mixed with other organic solvents at room temperature [**10**]. S, Se and Te form stable compounds with all elements, since they are non-metals. They also form good electrical insulators. Works on $AgFeS_2$ are more in literature in terms of fabrication, compared with $AgFeSe_2$ and $AgFeTe_2$. Leach [**11**] developed a colloidal hot-injection synthesis to obtain $AgFeS_2$ with spherical and bullet-like morphology. Through the ultraviolet-visible (Uv-Vis) absorbance spectrum, the bandgap value of the tetragonal, t-$AgFeS_2$ was estimated to be 1.06 eV, while the bandgap value of the orthorhombic, O-$AgFeS_2$, was estimated to be 1.20 eV. Zheng *et. al.,* [**2**] fabricated $AgFeS_2$-Nanowire, modified $BiVO_4$ photo-anodes for photoelectro-Chemical (PEC) water splitting, with a narrow bandgap value of 0.9 eV. Sciacca *et. al.,* [**12**] reported the synthesis of a semi-conducting $AgFeS_2$ nanowires obtained from the conversion of Ag nanowires. The optical measurement on nanowires ensemble confirmed the semi-conducting nature of $AgFeS_2$, with a direct bandgap 0f 0.88 eV. Han *et. al.,* [**13**] performed a facile one-pot colloidal route for controlled synthesis of ternary $AgFeS_2$ nanocrystals with a bandgap of 1.21 eV. Zhou *et. al.,* [**14**] employed a facile colloidal approach to synthesize $Ag_8(Ge_{1-x},Sn_x)(S_{6-y},Se_y)$ nanocrystals in a highly controlled way. By varying their chemical compositions, bandgap values of 0.88-1.45 eV was obtained. The Ag_8GeS_6 nanocrystals with an approximate bandgap of 1.45 eV were employed as a model light harvester to access their applicability to solar cells. In all these syntheses, there is sparse literature on the theoretical calculation of the electronic structures of these compounds.

In this study, the electronic band structure has been investigated for the compounds $AgFeS_2$, $AgFeSe_2$ and

$AgFeTe_2$ using LDA+U scheme within the density functional theory (DFT) to predict their energy bandgap values and other physical properties that have been observed experimentally.

Computational details

The ternary chalcopyrite crystallizes in the tetragonal structure I-42 *d* with space group number 122. The chalcopyrite is a superlattice of the Zinc-blende structure. The I-III-VI_2 form ternary compounds in which each group VI element [Sulphur (S), Selenium (Se), and Tellurium (Te)] is coordinated by two Silver (Ag) (group I) and two Iron (Fe) (group III) atoms. Each of the Fe atom is tetrahedrally bonded by four of either S, Se or Te depending on the compound. The Wyckoff's atomic coordinates for the three species of atoms in this structure are assigned the 4a for Fe, 4b for Ag and 8*d* for S, Se. A z value (the number of formula unit in a unit cell) of four was used in all the computations, this gave a total of 16 atoms per unit cell. The calculations were done using the Abinit package [**15,16**] which implements the pseudopotential method within the density functional theory (DFT). In this study, the structure optimization, electronic band structure, density of states (DOS) and partial density of states (PDOS), that is, the orbital decomposition of the various states in the DOS was carried out for $AgFeS_2$, $AgFeSe_2$ and $AgFeTe_2$. The first of these computations was the structure optimization. The aim here was to obtain the lattice parameter and lattice deformation parameter, U, and consequently, the atomic positions. The starting lattice parameters were adopted from the literature [**17,18**]. The tolerance on force was 0.01, the norm-conserving pseudopotentials were used in all the optimization computations. The results of the structure optimization are shown in **Table 1**, while the employed structure is displayed in **Fig. 1**. The projector augmented wave (PAW) was used in the LDA+U scheme in calculating the electronic band structure, and consequently, the total density of states and the partial density of states. Some of the parameter used in the computations includes an energy tolerance of 10^{-8}, a kinetic energy cutoff of 10 Ha and a Monkhorst-Pack shifted grid of 4x4x4.

Table 1. Lattice parameters and Wyckoff's atomic positions.

	Atoms	X	Y	Z	Sites	Lattice parameter (Bohr)	Lattice parameter Experiment (Bohr)
$AgFeS_2$	Ag	0.0	0.0	0.0	4a	a=10.2732, c=20.4980	a=10.2742[16], c=20.4987
	Fe	0.0	0.0	0.5	4b		a=10.7521[19], c=19.5011
	S	0.2857	0.25	0.125	8d		
$AgFeSe_2$	Se	0.1576	0.25	0.125	8d	a=10.8772, c=19.4654	a=12.4339[2], c=16.9312
$AgFeTe_2$	Te	0.3023	0.25	0.125	8d	a=10.8738, c=19.4592	

[17]Bindi *et. al.*, (2006)
[19]Eckerlin and Kandler (1971)

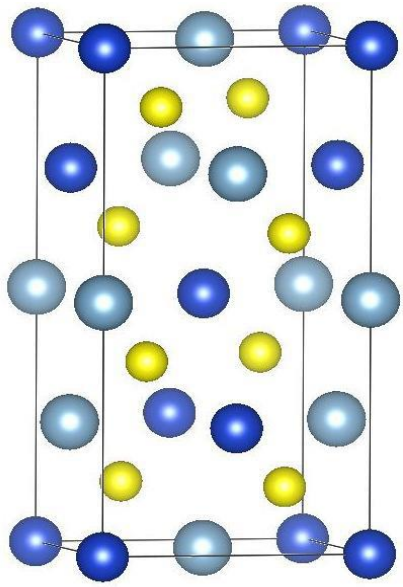

Fig. 1. The crystallographic structure used in the computations. Yellow balls represent S, Se or Te atoms, Blue balls for Ag atoms and Grey balls for Fe atoms.

Results and discussion

The electronic band structure of $AgFeS_2$, $AgFeSe_2$ and $AgFeTe_2$ are presented in **Fig. 2** to **Fig. 4** respectively. The plot is energy against high symmetry points in the first brillioun zone. The Fermi energy is at the zero mark in the plot. The valence band maximum (VBM) and the conduction band minimum (CBM) are at the gamma (r) points as shown in **Fig. 2** to **Fig. 4**, indicating that the bandgaps are direct. **Fig. 2** shows the band structure for $AgFeS_2$, the bands closest to the Fermi level are flat with narrow dispersion, as a result, the other transition points P, M and X are notable. The computations showed that the bandgap values for these materials are 3.33 eV, 0.05 eV and 1.3 eV for $AgFeS_2$, $AgFeSe_2$ and $AgFeTe_2$ respectively. This means that the three materials under investigation are semiconductors. The 3.33 eV obtained for $AgFeS_2$ is far above the experimental values of 1.06 eV and 0.9 eV reported [**11,2**]. A value of 0.88 eV was also reported [**12**]. Zhou *et. al.*, [**14**] reported a range of values from 0.88-1.45 eV. Theoretically, [**20**] reported a calculated bandgap value greater than 2.0 eV. This showed a level of agreement with this work.

Fig. 3 shows that $AgFeSe_2$ is a narrow band material with a bandgap value of 0.05 eV, but a value of 0.23 eV was reported experimentally while the calculated value was greater than 2.0 eV [**20**]. The bands around the Fermi level, when compared with those of $AgFeS_2$, it is seen that the bands of $AgFeSe_2$ are some worth more disperse that those of $AgFeS_2$. The band structure calculation for $AgFeTe_2$ yielded a bandgap value of 1.30 eV which agrees with the result reported by Kiselyova *et. al.*, [**20**]. Works on $AgFeSe_2$ and $AgFeTe_2$ are scarce in the literature. The values of important transition gaps and Comparison of results with other published works are tabulated in **Table 2**.

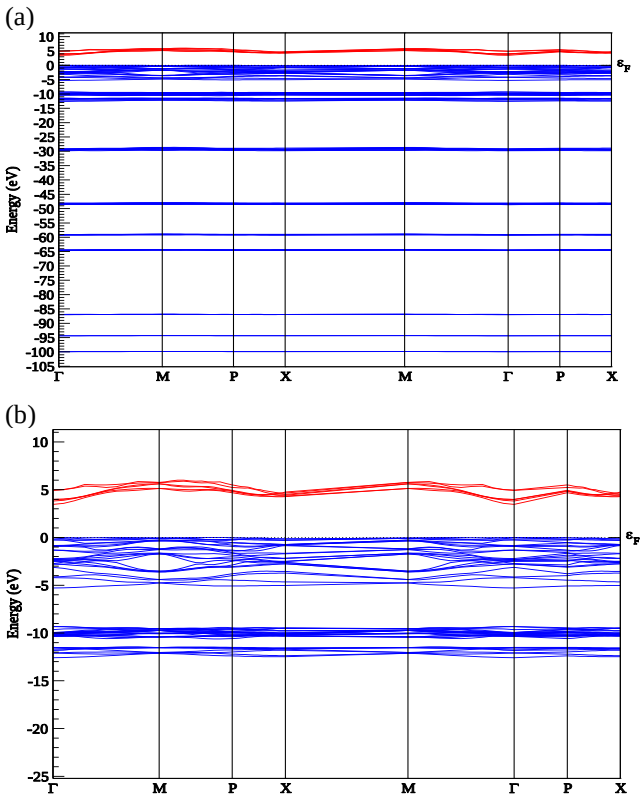

Fig. 2. Band structure of $AgFeS_2$, (a) shows the entire valence band (b) shows the bands close to the Fermi level.

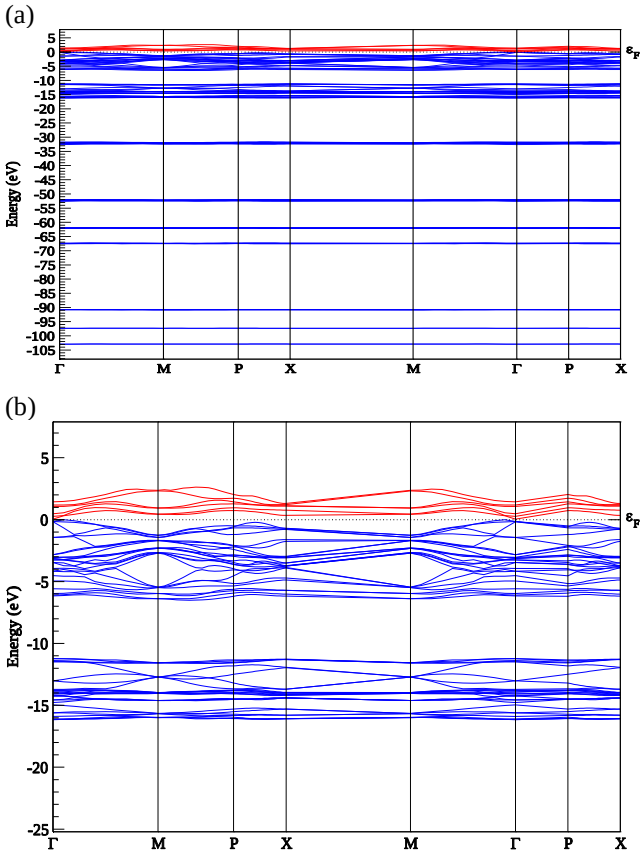

Fig. 3. Band structure of $AgFeSe_2$, (a) shows the entire valence band (b) shows the bands close to the Fermi level.

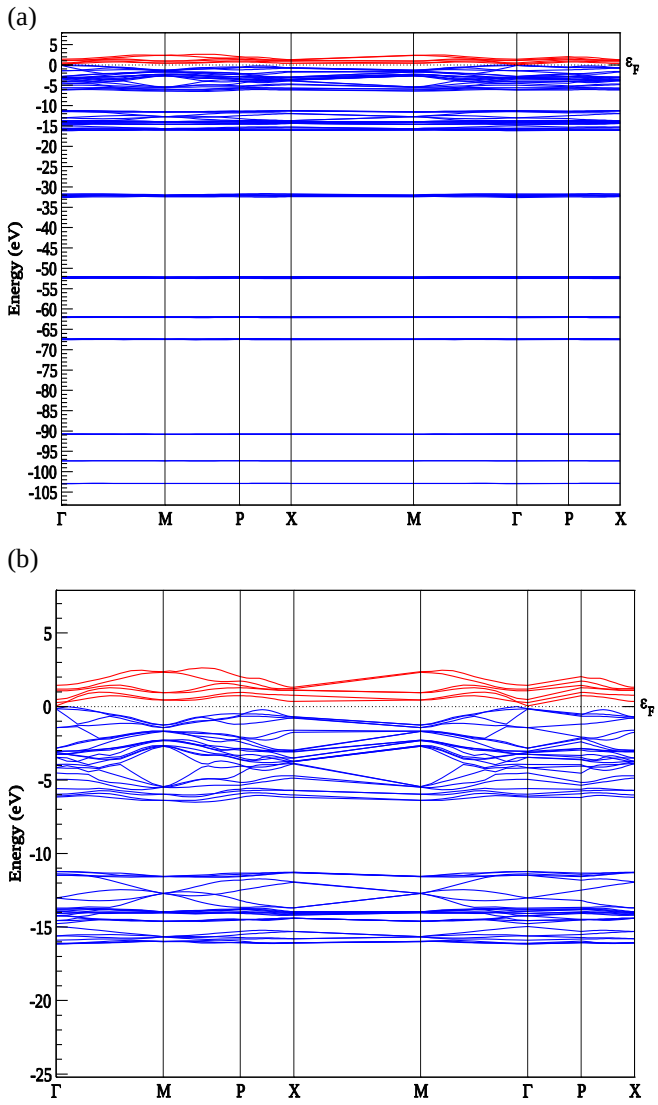

Fig. 4. Band structure of $AgFeTe_2$, (a) shows the entire valence band (b) shows the bands close to the Fermi level.

Table 2. Comparison of important transition gaps and Comparison of results with other published works

	(eV)	(eV)	(eV)	(eV)
$AgFeS_2$	3.33[a], 2.00[g]	5.0[a]	4.58[a]	4.17[a]
Experiment	0.9[b], 1.06-1.20[c], 0.88[d], 1.21[e], 0.88-1.45[f],	-	-	-
$AgFeSe_2$	0.05[a], 2.0[g]	0.39[a]	0.67[a]	0.47[a]
Experiment	0.23[g]	-	-	-
$AgFeTe_2$	1.30[a]	2.37[a]	3.42[a]	2.11[a]
Experiment	-	-	-	-

[a]Current work
[b]Ref. 2
[c]Ref. 11
[d]Ref. 12
[e]Ref. 14
[g]Ref. 20

Fig. 5 to **Fig. 7** represent the plot of the total density of states (DOS) against the energy in Hartree. The Fermi energy is at 0.16 Ha, 0.27 Ha and 0.03 Ha for $AgFeS_2$, $AgFeSe_2$ and $AgFeTe_2$ respectively. The bandgaps are well reproduced and clearly seen at the Fermi level, reinforcing the fact that the materials are semiconductors, hence they can be used in developing environmentally sustainable processes and devices such as solar cells and optoelectronics. The various orbital components of the density of states for the atoms of the compounds are obtained from the partial density of states plots presented in **Fig. 8** to **Fig. 10**. The valence states included in the calculations are Ag: 4*s*, 4*p*, 4*d* and 5*s*; Fe: 3*s*, 3*p*, 3*d* and 4*s*; S: 3*s*, 3*p*; Se: 4*s*, 4*p*; Te: 5*s*, 5*p*. **Fig. 8(a)** to **Fig. 8(c)** show the orbital decomposition for Ag, Fe and S in $AgFeS_2$. The states represented by the peak close to the -3 Ha mark are that of Ag-4s while those of the Ag-5s are a small fraction of states immediately before the Fermi energy, and also a fraction of the conduction band. These are as shown in **Fig. 8**. Also, from **Fig. 8(a)**, the Ag-4*d* states are dominant about -0.17 to -0.22 Ha. The contribution from Ag-4*p* represents peak about -1.58 Ha. The partial density of states representing states of the Fe atoms is displayed in **Fig. 8(b)**. The Fe-3*d* states are shown by the density of states at the -3.5 Ha, thus, Fe-3*d* dominates here.

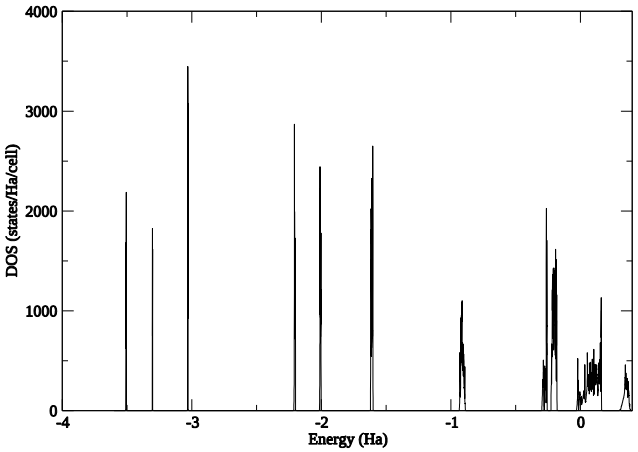

Fig. 5. Total density of states for $AgFeS_2$

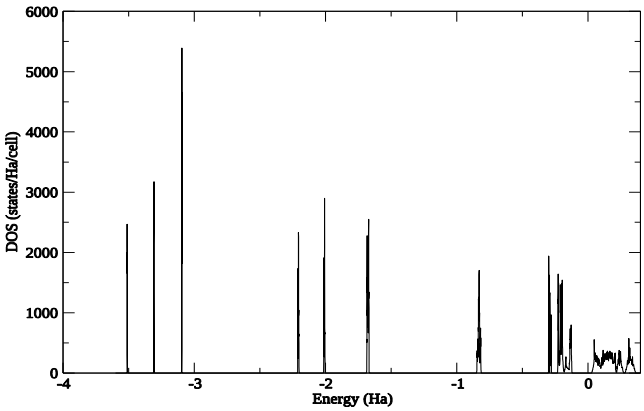

Fig. 6. Total density of states for $AgFeSe_2$

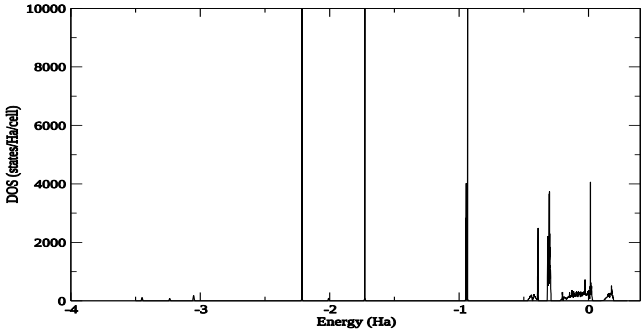

Fig. 7. Total density of states for $AgFeTe_2$

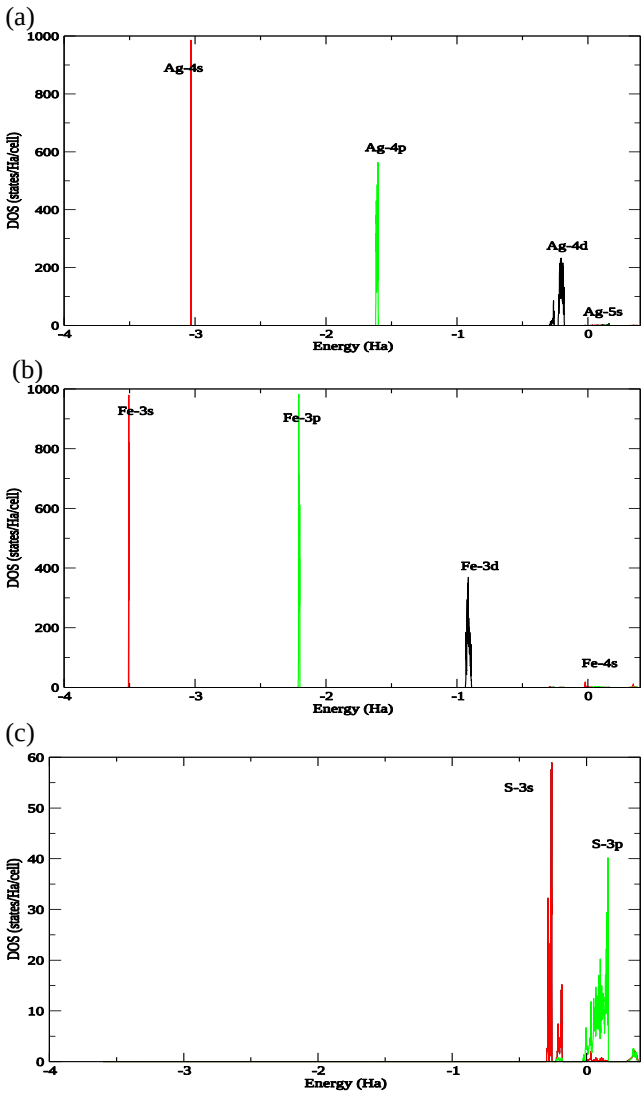

Fig. 8. The partial DOS of $AgFeS_2$ from Ag, Fe and S atoms. (a) partial DOS from Ag (b) partial DOS from Fe (c) partial DOS from S.

The Fe-4*s* state is shown as small curves and peaks both around the VBM and CBM. The Fe-4*p* is at higher energy levels compared to the Fe-3*s*. The Fe-4*p* states are the dominant states about -2.19 Ha. The states close to -1Ha are those of the Fe-3*d* orbitals, as expected, they occupy higher energy levels compared with Fe-3*s* and Fe-3*p*. From **Figs. 8(a)** and **8(b)**, the Ag-4*d*is higher in the energy spectrum than Fe-3*d*. This is also as expected. The

conduction band is dominated by Fe-4*s* orbitals. The states directly below the Fermi level are S-3p dominated, this is as seen from **Fig. 8(c)**. The partial density of states plot also showed the S-3*s* represented by the peaks and curves about -0.22 to 0.17Ha. From the graphs, Ag-4*d* and S-3*s* occupy this energy range. **Fig. 9(a)** to **Fig. 9(c)** display the various orbital contributions to the total DOS of $AgFeSe_2$ from the constituent atoms. **Fig. 9(a)** shows the partial DOS of the Ag atoms, the 4*s*, 4*p*, 4*d* and 5*s* orbital contributions are also shown. From the graph, Ag-4*s* state is shown by the undispersed peak near -3 Ha while the Ag-5*s* state contribution is seen at the energy range of -0.29 to 0.27 Ha. The energy range of -0.29 to -0.17Ha is predominantly made up of Ag-4*d* and Se-4*p* states. Some fraction of the conduction bands are also of the Ag-4*d*. The peak at -1.7 Ha is contributed by Ag-4*p*. **Fig. 9(b)** is the partial DOS for the Fe atoms. The conduction band is made up predominantly of the Fe-4*s* and Se-4*p* states with a small fraction of Se-4*p* states as seen from **Fig. 9(c)**.

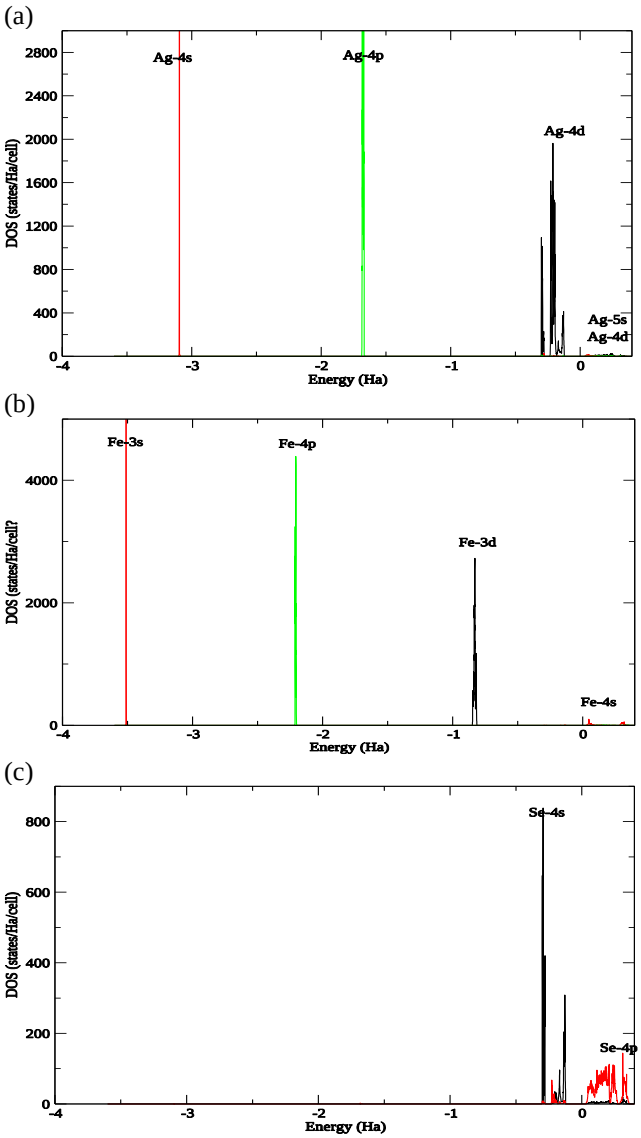

Fig. 9. The partial DOS of $AgFeSe_2$ from Ag, Fe and Se atoms. (a) partial DOS from Ag (b) partial DOS from Fe (c) partial DOS from Se.

The bands immediately preceding the Fermi energy are dominated by Fe-4*s* and Se-4*p* states. The Fe-3*d* and Fe-3*p* are responsible for the peaks at -0.8 Ha and -2.2 Ha respectively. The partial DOS for $AgFeTe_2$ are shown in **Fig. 10(a)** to **Fig. 10(c)** for Ag, Fe and Te respectively. The Ag-4*s*, Ag-5*s*, Ag-4*p* and Ag-4*d* are presented in **Fig. 10(a)**. States close to the -3 Ha mark represent contribution from Ag-4*s*, while the peak at -1.7 Ha is for the Ag-4*p* orbitals. Contributions of Ag-4*d* to the total DOS is shown by curves of energy range -1.0 to the Fermi level, and some of the conduction bands are of Ag-4*d* states. The Ag-4s orbital is packed about the Fermi level and conduction band. Most of the states around -1.0 Ha are Fe-3*d*, the Fe-3*p* are at -2.2Ha as seen in **Fig. 10(b)**. From **Fig.10(a)** and **Fig.10(b)**, it is clearly seen that the states about the Fermi level are composed of Ag-4*d*, Fe-4*s*, Te-3*p* and Te-3*s*, but Te-3*p* states are dominant about -0.25 Ha to the Fermi energy.

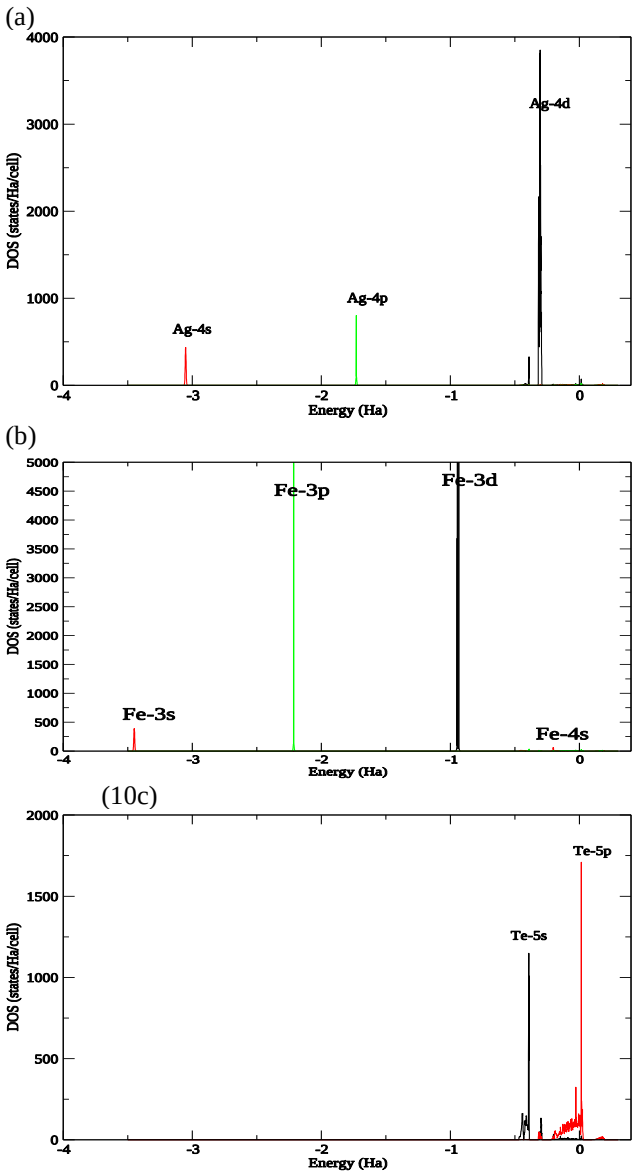

Fig. 10. The partial DOS of $AgFeTe_2$ from Ag, Fe and Se atoms. (a) partial DOS from Ag (b) partial DOS from Fe (c) partial DOS from Te.

Conclusion

The electronic properties of the Chalcopyrite $AgFeS_2$, $AgFeSe_2$ and $AgFeTe_2$ have been investigated using the pseudopotential method within the density functional theory (DFT). The LDA+U technique and the projector augmented wave (PAW) were used for the electronic band structure calculations, while the norm-conserving pseudopotentials were used for the structure optimization. The calculated results showed that $AgFeS_2$, $AgFeSe_2$ and $AgFeTe_2$ are p-type semiconductors with energy bandgap values of 3.33 eV, 0.05 eV and 1.30 eV respectively. The transition points in the band structure are all notable because of the narrowness of the bands about the Fermi level. The total density of states and their corresponding partial density of states were also computed. The Fe-4*s* state dominates the $AgFeS_2$ conduction band while S-3*p* dominates the valence band preceding the Fermi level. The conduction band for $AgFeSe_2$ is dominated by Se-4*p* and Fe-4*s* states while the valence band is predominantly Se-4*p* and Ag-4*d*. For $AgFeTe_2$, the dominant valence state is the Te-5*p* states. More works need to be done to ascertain the correct banger values of these materials because of the inconsistencies between these results and experimental values.

Keywords

$AgFeS_2$, $AgFeSe_2$, $AgFeTe_2$, electronic band structure, chalcopyrite materials.

Received: 09 April 2020
Revised: 20 April 2020
Accepted: 22 September 2020

References

1. Zhong, H.; Bai, Z.; Zou, B.; *J. Phys. Chem. Lett*, **2012**, *3*, 3167.
2. Zheng, X.; Sciacca, B.; Garnett, E.C.; Zhang, L.; *Chem plus Chem*, **2016**, *81*, 1075.
3. Enderby, J.E.; Barnes, A.C.; *Rep. Prog. Phys*, **1990**, *53*, 85.
4. Kirchhoff, F.; Holeder, J.M.; Gillan, M.J.; *EPL*, **2018**, *33*, 1.
5. Gershon, T.; Gokman, T.; Gunawan, O.; Haight, R.; Guha, S.; Shin, B.; *MRS Commun.*, **2014**, *4*, 159.
6. Scragg, J.J.; Larsen, J.K.; Kumar, M.; Persson, C.; Sandler, J.; Siebentrict, S.; Bjorkman, C.; *Phys. Status Solidi* (B), **2016**, *253*, 247.
7. Fang, C. M.; De Groot, R. A.; Weigers G. A.; *J. Phys. Chem. Solids*, **2002**, *63*, 457.
8. Gershon, T.; Sardashti, K.; Lee Y. S.; Gunawan, O.; Singh S.; Bishop D.; Kummel, A. C.; Height, R.; *Acta Mater*., **2017**, *126*, 383.
9. Bhattacharyya, B.; Pandey, A.; *J. Am. Chem. Soc.*, **2016**, *138*, 10207.
10. World Intellectual Property Organization (WIPO) (**2006**). Processes for preparing chalcopyrite-type compounds and other inorganic compounds. International Search Report. WO 2006/119621 AI.
11. Leach A. D. P.; The Phase Dependant Optoelectronic Properties of Ternary I-III-VI_2 Semiconductor Nanocrystals and their Syntheses. Ph.D Thesis, **2017**, 121-143.
12. Sciacca B.; Yalcin A. O.; Garnett E.C.; *J. Am. Chem. Soc.*, **2015**, *137*, 4340.
13. Han S. K.; Gu, C. M.; Wang Z. M.; Yu, S. H.; *Heterochimers*, **2013**, *9*, 3765.
14. Zhou B.; Xing Y.; Miao, S.; Li, M.; Zhang W. H.; Li C.; Synthesis and characterization of Ag_8 $(Ge_{1-X}, Sn_x)(S_{6-y},Se_y)$ Colloidal Nanocrystals. *Chem.*, **2014**, *20*, 12426.
15. Gonze, X.; Beuken, J.M.; Caracas, R.; Detraux, F.; Fuchs, M.; Rignanese, G.M.; Sindic L.; Verstraete, M.; Zerah, G.; Jollet, F.; Torrent, M.; Roy, A.; Mikami, M.; Ghosez, P.H.; Raty, J.Y.; Allan, D.C.; *Comput. Mater. Sci.*, **2002**, *25*, 478.
16. Gonze, X.; Rignanese, G.M.; Verstraete, M.; Beuken, J.M.; Pouillon, Y.; Caracas, R.; Jollet, F.; Torrent, M.; Zerah, G.; Mikami, M.; Ghosez, P.H.; Veithen, M.; Raty, J.Y.; Olevano, V.; Bruneval, F.; Reining, L.; Godby, R.; Onida, G.; Hamann, D. R.; Allan D. C.; *Z. Kristallogr*, **2005**, *220*, 558.
17. Bindi L.; Spry P. G.; Pratesi G.; *Canad. Mineral.*, **2006**, *44*, 207.
18. Madelung, O.; Semiconductors: Data Handbook, Springer, 3rd Edition, **2004**, pp293.
19. Eckerlin, P.; Kandler, H.; Structure, Data of Elements and Intermetallic Phases. Springer, New York, **1971**.
20. Kiselyova, N. N.; Dudarev, V. A.; Korzhuyev, M. A.; *Appl. Res.*, **2016**, *7*, 34.